Uncertainty and capability of quantitative EPMA at low voltage – A review

2012 IOP Conf. Ser.: Mater. Sci. Eng. 32 012016

(http://iopscience.iop.org/1757-899X/32/1/012016)

IOP Conf. Series: Materials Science and Engineering **32** (2012) 012016 doi:10.1088/1757-899X/32/1/012016

Uncertainty and capability of quantitative EPMA at low voltage – A review

C Merlet[1,3] **and X Llovet**[2]
[1] Université de Montpellier II, CNRS, Laboratoire Géosciences Montpellier, Place Eugène Bataillon, FR-34095 Montpellier Cedex 5, France
[2] University of Barcelona, Centres Científics i Tecnològics (CCiT), C/ Lluís Solé i Sabarís 1-3, ES-08028 Barcelona, Spain

E-mail: merlet@gm.univ-montp2.fr

Abstract. The use of electron probe microanalysis (EPMA) at low voltage allows improvements in the lateral resolution and surface sensitivity of the technique down to the sub-micrometre scale, and it is also useful in minimizing X-ray absorption (for the analysis of ultra-light elements), charging effects and secondary fluorescence. However, EPMA at low voltage is accompanied by a number of problems which may affect the accuracy of quantitative results. A large number of these problems arise from the need of using low-energy X-ray lines such as L- and M-lines, which have low fluorescence yields, large uncertainties in the mass attenuation coefficients, and are affected by several spectroscopic difficulties (e.g., peak shifts and overlaps). Other factors that play an important role at low voltage are carbon contamination, surface oxidation, the quality of sample polishing, the influence of a conductive coating and the limitations of matrix correction procedures. In this paper, we illustrate the capabilities of EPMA at low voltage and we examine in detail the different sources of uncertainty that may affect the accuracy of quantitative results.

1. Introduction

The incorporation of the field emission gun (FEG) in the scanning electron microscope (SEM) and, more recently, in the electron microprobe, has stimulated the operation of these instruments at low voltage. Using FEG electron sources, it is possible to obtain a finely focussed (< 100 nm) electron beam with relatively high current (< 100 nA) even at low beam energies (< 5 keV). At such energies, the penetration range of incident electrons drops from the conventional micron scale down to the sub-micrometre scale, and leads to a significant improvement in the lateral resolution and surface sensitivity of electron probe microanalysis (EPMA) [1]. This opens a wide range of new possibilities for the characterisation of materials that are heterogeneous on a sub-µm scale. The operation of EPMA at low voltage is also useful for the analysis of ultra-light elements, as it largely reduces X-ray absorption (the main source of uncertainty for such elements), for a number of insulating materials, as charge compensation effects allows to analyze them without any conductive coating [2], and the analysis near phase boundaries, as it reduces secondary fluorescence effects.

However, EPMA at low-beam energies is accompanied by experimental and analytical problems which may affect the accuracy of quantitative results [3]. At low-beam voltages, low-energy X-ray

[3] To whom any correspondence should be addressed.

lines such as L- and M-lines have to be used, and these lines are often affected by spectroscopic difficulties (peak shifts and overlaps) and larger uncertainties in the associated mass attenuation coefficients (MACs). Moreover, the fluorescence yields for the L- and M-lines are generally lower than for the conventional K-lines. As a result, peak-to-background ratios are also lower and the detection limit worsens. At low voltage, the overvoltage ratio, defined as $U = E_0/E_c$, where E_0 is the beam energy and E_c is the critical excitation energy of the considered line, may also be relatively low (< 2), decreasing significantly the X-ray intensity. Also, the approximations underlying matrix corrections procedures (e.g., $\phi(\rho z)$ models) at low voltage are not well established. For instance, the validity of expressions used in conventional correction procedures for the calculation of quantities such as the ionisation cross-section or the stopping power at low voltages (or close to the ionisation threshold) may be questioned. Finally, at low beam voltages, a surface layer of several nanometres in thickness represents a much larger fraction of the sample and, therefore, the influence of carbon contamination, surface oxidation, the quality of the sample polish or a conductive coating becomes more significant. Here, measurements at multiple voltages may become useful to separately characterize a sample substrate under a layer or multiple layers, using suitable thin film programmes [4].

In this paper, we illustrate the advantages of the use of EPMA at low voltage by means of several examples and we examine the difficulties that may affect the accuracy of quantitative results.

2. Analytical resolution of EPMA

Figure 1 shows the trajectories of electrons in Si, computed by using Monte Carlo simulations, for different electron incident beam energies. We can see that the penetration range of electrons reduces as the beam energy decreases.

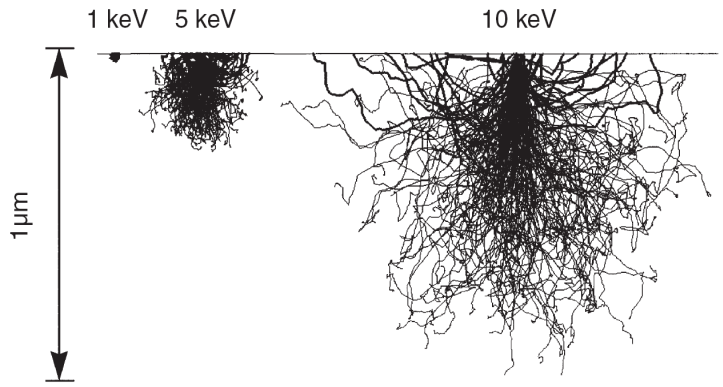

Figure 1. Electron trajectories in Si with E = 1, 5 and 10 keV, computed using Monte Carlo simulations.

The spatial resolution of EPMA can be estimated from the effective ionisation range of electrons R_x, or X-ray range, defined as the average path length that electrons travel before slowing down to an energy equal to the critical excitation energy of the considered electron shell. The ionisation range can be estimated by means of a simple relationship [5]:

$$\mathrm{R_X\,(nm)} = \frac{33.A}{\rho.Z}\left(E_0^{1.7} - E_c^{1.7}\right) \qquad (1)$$

where E_0 and E_c are expressed in keV, A is the atomic weight (in g/mol), Z is the atomic number, and ρ is the density (in g/cm^3). Here it should be noted that the beam diameter needs also to be taken into account to estimate the spatial resolution, especially at low beam energies.

Table 1 lists X-ray ranges calculated by using Eq. (1) for Fe Kα (E_c = 7.11 keV) and Fe Lα (E_c = 0.707 keV) X-rays emitted from C, Si, Fe and Au, and for incident electron energies in the range 2.5 - 30 keV. Notice that Fe is considered here as a ``trace'' element immersed within C, Si, Fe and Au matrices. At 20 keV, the effective ionisation range for Fe Kα ranges from 3.9 μm for C to 470 nm for Au, which would correspond to the conventional μm-scale spatial resolution of EPMA. However, at 2.5 keV, the effective ionisation range for Fe Lα drops substantially and goes from 123 nm for C down to 18 nm for Au. The improvement in spatial resolution at 2.5 keV is worth noticing. We also note that, the overvoltage ratio for the Fe Kα-line is above 2 for conventional beam energies (> 15 keV), but it drops below 2 for beam energies lower than 12 keV.

Table 1. X-ray range (in μm) calculated from Eq. (1) for Fe Kα (E_c = 7.11 keV) and Fe Lα (E_c = 0.707 keV) in C, Si, Fe and Au matrices and beam energies in the range 2.5 - 30 keV.

		X-ray range							
		Fe Kα-line (E_c = 7.11 keV)					Fe Lα-line (E_c = 0.707 keV)		
Matrix	keV	E_0 = 30	E_0 = 25	E_0 = 20	E_0 = 15	E_0 = 10	E_0 = 10	E_0 = 5	E_0 = 2.5
	Density (g/cm^3)	U_0=4.2	U_0=3.5	U_0=2.8	U_0=2.1	U_0=1.4	U_0=14	U_0=7	U_0=3.5
C	2.26	8.66	6.13	3.94	2.10	0.645	1.45	0.435	0.123
Si	2.32	8.46	5.98	3.84	2.04	0.629	1.41	0.424	0.120
Fe	7.86	2.67	1.76	1.13	0.603	0.199	0.447	0.134	0.038
Au	18.85	1.29	0.74	0.47	0.252	0.096	0.216	0.065	0.018

3. Advantages of EPMA at low voltage

3.1. Quantification of thin films and multilayers

The first benefit of using EPMA at low voltage is the improvement in surface sensitivity, which is useful for the analysis of very thin over-layers.

EPMA was originally developed for the analysis of bulk samples (i.e., those samples that are homogeneous both laterally and in depth at the μm-scale) but it was later extended so as to allow the analysis (composition and thickness) of thin layers with thicknesses below 1 - 2 μm [4]. Such improved depth resolution is achieved mainly because the depth distribution of X-ray production can be predicted within a reasonable accuracy by using an analytical $\phi(\rho z)$ model. Analysis of thin layers by EPMA requires in many cases the measurement of X-ray intensities (*k*-ratios) at different electron incident energies and the use of a thin film programme which determines the layer thickness and composition by fitting the predictions of the $\phi(\rho z)$ model to the measured *k*-ratios (see figure 2).

The optimal choice of accelerating voltage and X-ray line for the analysis of thin layers and multilayers depends strongly on the dimension of the multilayered structure: the lower the incident electron energy, the shallower the electrons penetrate into the specimen and, as a result, the *k*-ratio becomes more sensitive to resolve structures on the sub-μm scale.

This is illustrated in figure 2, which shows the variation of the *k*-ratio for Ti and Si Kα X-rays, as a function of beam energy, emitted from a Si 17 μg/cm^2 / Ti 18 μg/cm^2 bi-layer on Si. In this example, *k*-ratio measurements at 3 and 4 keV are essential to infer the correct near-surface configuration of the sample. If measurements are only carried out above 5 keV, it becomes almost impossible to predict that a Ti layer is buried under Si [6]. This example illustrates that measurements at low voltage are essential to determine the near-surface structure of stratified samples.

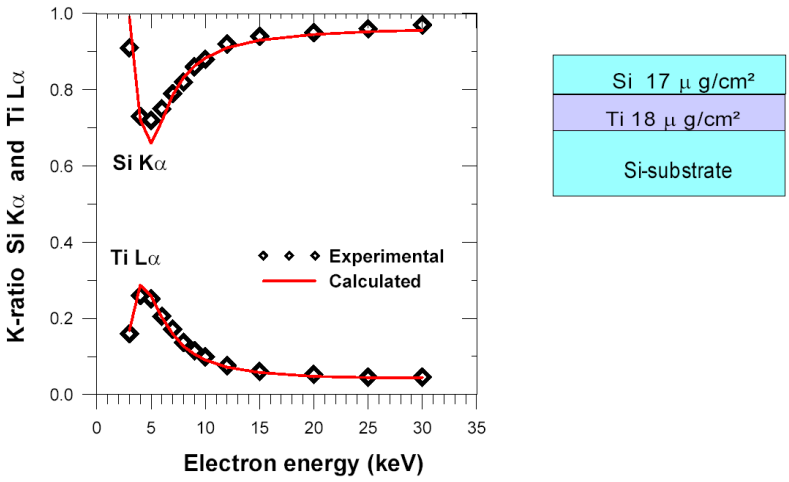

Figure 2. Comparison between calculated and measured *k*-ratios for Si Kα and Ti Kα as a function of beam energy from a Si 17 μg/cm^2 / Ti 18 μg/cm^2 bi-layer on Si. Symbols are experimental data measured by Bastin et al. [6]. Continuous lines are the predictions of X-FILM [4].

3.2. Quantification of ultra-light elements

As mentioned previously, EPMA at low voltage reduces the effective ionisation range of electrons and, as a consequence, X-ray absorption is also reduced. This potentially improves the accuracy of quantitative analysis for ultra-light elements, for which the uncertainties in the MACs are much more important relatively to more energetic lines (in some cases these uncertainties may be of 1000 %).

Figure 3 illustrates the effect of the uncertainty in the MAC of O Kα in TiO_2 on the O-concentration as calculated with the X-PHI model [7]. For the considered MAC uncertainties (from 0 % up to 10 %), the maximum error in the O-concentration is obtained at a beam energy of approximately 15 keV. Above 15 keV, the error in the concentration becomes relatively constant, with a value similar to the MAC uncertainty. However, below 15 keV, the effect of the MAC uncertainty on the O-concentration is significantly reduced. For example, at 5 keV, the error in the O-concentration drops to 4 %, even if the MAC uncertainty is 10 %. Notice the MAC of O Kα in Ti adopted in X-PHI (20000 cm^2/g) is slightly lower than the value reported in Henke's tabulation (22100 cm^2/g) [8]. This difference is most likely due to the effect of chemical bonding (see below) and experimental uncertainties affecting Henke's database. Similar discrepancies are also found in other MAC tabulations obtained from EPMA measurements.

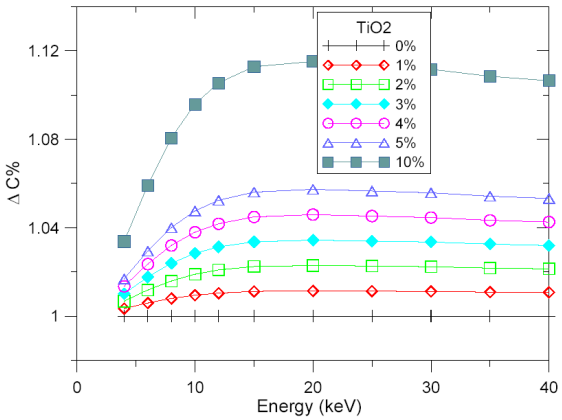

Figure 3. Relative error in the O-concentration (ΔC%) in TiO_2 for different uncertainties in the MAC of O Kα, ranging from 0 % up to 10 %, as a function of beam energy.

3.3. Improvement in spatial resolution

The development of the FEG-SEM and, more recently, the FEG electron microprobe, has made it possible to achieve finely focused (< 100 nm) electron beams with a relatively high currents (< 100 nA) even at low beam energies (< 5 keV). At such energies, the X-ray range drops from the conventional µm-scale down to the sub-µm range permitting the acquisition of -ray maps and point analyses with sub-micron resolution. FEG-EPMA fills the gap existing between conventional EPMA (with µm resolution) and X-ray analysis in the transmission electron microscope (with nanometre resolution).

To illustrate the improvement in lateral resolution that can be achieved at low voltage, X-ray maps were acquired on a sample consisting of hematite-ilmenite-rutile using a Jeol 8500F FEG electron microprobe and were compared to the results obtained with a conventional Cameca SX-100 electron microprobe [9]. Figure 4 shows Nb Lα, Fe Kα, Ti Kα X-ray maps, as well as the backscattered (BSE) electron image, of an area approximately 15x15 µm^2 in size acquired at 15 keV using the conventional microprobe and Nb Lα, Fe Kα, Ti Kα maps of approximately the same region obtained at 6 keV using the FEG electron microprobe. The improvement in lateral resolution is worth noticing, especially for Nb. This is also illustrated in table 2, which tabulates the X-ray range and the lateral resolution, in ilmenite calculated by using Eqs. (1) and (2) for the different X-ray lines used in the maps, at E_0 = 15 keV and E_0 = 6 keV. The mass density of ilmenite is in the range of 4 - 5 g/cm^3. The X-ray range is also computed for Zr Lα. The lateral resolution, R_S, can be obtained using the simple formula

$$R_S = \sqrt{4(R_x - Z_m)^2 + d_0^2}\,, \qquad (2)$$

which requires knowledge of the X-ray range (R_x), the depth of the maximum of the X-ray depth distribution (Z_m) and the beam diameter (d_0). A beam diameter of 100 nm was used in table 2.

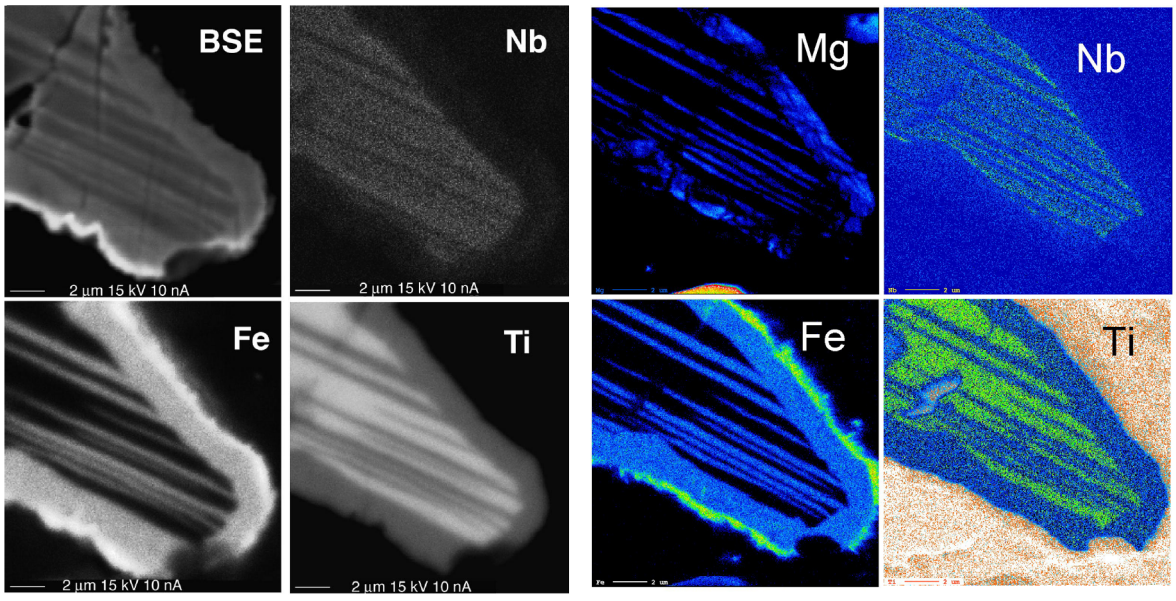

Figure 4. X-ray maps for the distribution of Mg, Nb, Fe and Ti in a sample consisting of hematite-ilmenite-rutile. a) Results obtained with a conventional Cameca SX-100 electron microprobe at 15 keV [9] (the BSE image is also shown). b) Results obtained with a Jeol 8500F FEG electron microprobe at 6 keV.

Table 2. X-ray range (in μm) and lateral resolution (R_S) for Mg Kα, Ti Kα, Fe Kα and Lα, Zr Lα and Nb Lα X-rays from ilmenite at 15 keV and 6 keV, based on Eqs. (1) and (2).

		E_0 = 15 keV					E_0 = 6 keV		
X-ray line	E_c keV	U_o (E_0/E_c)	Range	R_S	X-ray line	E_c keV	U_o (E_0/E_c)	Range	R_S
Mg Kα	1.3	11.5	1.30	1.95	Mg Kα	1.3	4.6	0.257	0.399
Ti Kα	4.97	3.0	1.12	1.68	Ti Kα	4.97	1.2	0.077	0.171
Fe Kα	7.11	2.1	0.95	1.43	Fe Lα	0.71	8.5	0.271	0.418
Zr Lα	2.22	6.8	1.27	1.90	Zr Lα	2.22	2.7	0.227	0.354
Nb Lα	2.37	6.3	1.26	1.90	Nb Lα	2.37	2.5	0.221	0.346

In order to examine the resolution achieved at low voltage, X-ray line scans were further acquired across the hematite-ilmenite-rutile at an energy of 6 keV and beam current of 15 nA, using the FEG electron microprobe. For comparison purposes, similar X-ray line profiles were obtained at 15 keV using a conventional electron microprobe. Figure 5 shows the X-ray line scans, of approximately 14 μm in length, corresponding to Mg and Ti Kα, and Zr, Fe and Nb Lα X-rays, as a function of the distance along the line. The location of the line profiles (white line superimposed on the Fe map) is also shown.

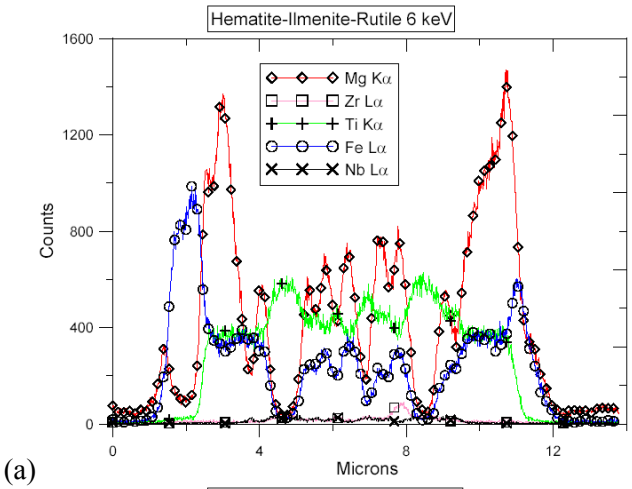

(a)

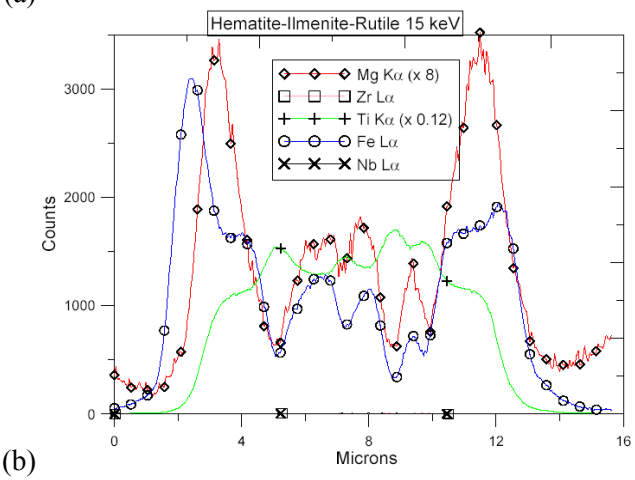

(b)

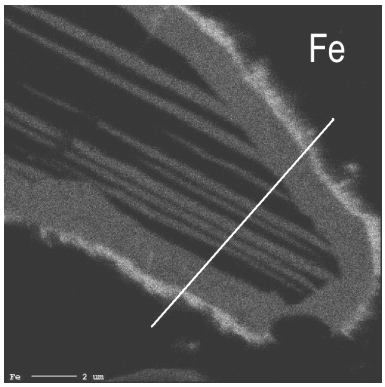

Figure 5. X-ray line scans across the hematite-ilmenite-rutile sample obtained with a FEG electron microprobe at 6 keV (a), and with a conventional electron microprobe at 15 keV (b). To facilitate comparison, the Ti and Mg profiles obtained at 15 keV have been multiplied by a factor of 0.12 and 8, respectively. The location of the line scan is shown on the Fe map.

It should be noted that the X-ray line scans shown in figure 5 are qualitative in nature, and therefore, counting rates are not proportional to element concentration. For instance, the counting rates measured on the ilmenite phase for Ti, Mg and Fe shown in figure 6a (400, 1300 and 400 counts/s, respectively) do not actually reflect the differences in concentration of these elements (TiO_2 62 wt%; MgO 20 wt%; FeO 18 wt%) [9]. This is so because X-ray counting rates depend not only on sample composition but also on other factors such as the overvoltage ratio or spectrometer efficiency.

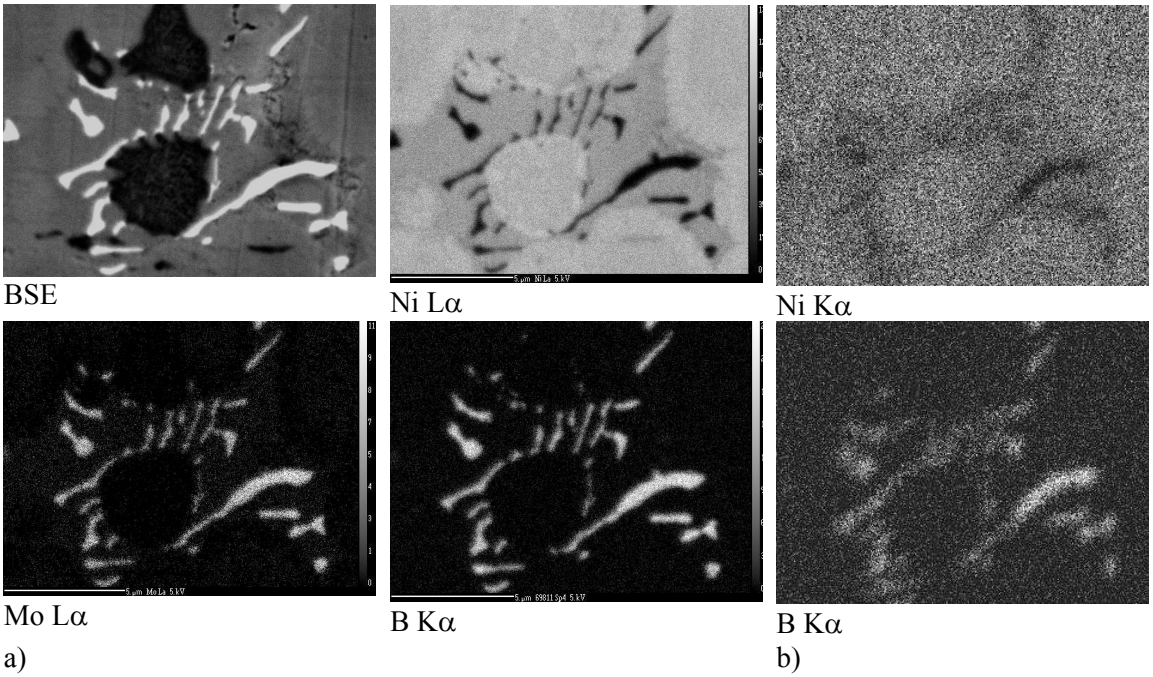

Figure 6. X-ray maps for the distribution of Ni, Mo and B in a Ni-base superalloy sample. a) Results obtained with a Cameca SX-Five FEG electron microprobe at 5 keV. b) Results obtained with a conventional Cameca SX-100 microprobe at 10 keV [10].

The width from 10 % to 90 % of the maximal intensity of a line scan across a sharp interface can be used as a measure of the lateral resolution. For the hematite-ilmenite interface, the lateral resolution of the Ti Kα- and Fe Lα-lines is 290 nm and 390 nm, respectively. Notice that, in this case, the resolution of the Ti Kα-line is slightly lower than that of the Fe Lα radiation mainly because at 6 keV, the Ti K-shell is excited at a very low over-voltage ratio (U = 1.2), which makes the X-ray range to drop drastically (see table 2). In comparison, the Ti Kα intensity measured at 15 keV (figure 5b) is 20 times higher. Notice that at 15 keV the rutile phase cannot be distinguished from the ilmenite phase.

A second example concerns the analysis of sub-micron borides occurring in Ni-base superalloys. In this case, X-ray maps of Ni, Mo and B were acquired at 5 keV and 40 nA using a Cameca SX-Five FEG electron microprobe, and the results were compared to those obtained earlier with a conventional Cameca SX-100 electron microprobe [10]. In the latter case, the maps had been obtained with a beam voltage of 10 kV and a beam current of 1 nA, in order to achieve the best possible resolution. The area scanned was approximately 14×14 μm^2 in size. In the case of the FEG microprobe, the analyzed X-ray lines were Ni Lα, Mo Lα and B Kα, while for the conventional microprobe, Ni Kα- and B Kα-lines had been used. The improvement in image resolution is demonstrated, especially for

boron. The use of FEG microprobes opens new possibilities for X-ray mapping at high spatial resolution.

3.4. Reduction of fluorescence effects

Another benefit of using EPMA at low-voltage is the reduction of secondary fluorescence near the boundary between two phases. Secondary fluorescence may lead not only to erroneous quantitative results but also to qualitative misinterpretation [11], especially in trace element analysis (and the two adjacent phases have similar atomic number). In our hematite-ilmenite-rutile example, EPMA analyses for Ti performed at 15 keV at the hematite phase shows systematically small Ti-contents. However, if the analyses are performed at 6 keV, no Ti is detected. This is so because at 6 keV, the main source that produces secondary fluorescence, namely Fe Kα X-rays, cannot be excited.

3.5. Quantification of insulating materials

In EPMA, analysis of insulators is typically performed by coating the sample with a conductive layer, generally C or Au, to prevent charging effects. However, in some materials, charge self-compensation can be achieved by suitably reducing the beam voltage. The principle is similar to that used for imaging insulators in the FEG-SEM without conductive coating. A beam voltage (usually between 2 - 3 keV) can be tuned such that the injected charge from the electron beam is compensated by the secondary and backscattered electrons leaving the specimen. To do that, knowledge of the potential at the sample surface is required, which can be determined by measuring the Duane-Hunt limit when charge compensation is reached [2].

Figure 7 shows the variation of O and Al *k*-ratio, as a function of measuring time, from a non-coated sapphire sample (Al_2O_3) with a beam voltage of 2.5 kV. The measurements were performed at the same sample position for almost 2 h, with an electron beam of 500 nA of current and 20 µm in diameter. The stability with time of the measured Al and O *k*-ratios is worth noticing. It would not be possible to achieve such stability at higher beam energy due to charging effects. The sample was plasma etched before the measurements and an O_2-jet was used to minimize C contamination during measurements. In spite of this, a decrease in X-ray intensity at a t = 80 min is observed which corresponds to the effect of C contamination after a beam shift (of approximately 5 µm) most likely due to charge implantation in the sample (second-order backscattered electrons). By measuring C Kα X-rays simultaneously with Al and O, the loss of X-ray intensity could be estimated to correspond to a 1.4 nm thick C layer (see section 4.2.4). We note that the (uncorrected) *k*-ratios are close to the nominal concentrations (O 47 wt%; Al 53 wt%), despite the high MAC of O Kα in Al (6700 cm^2/g). We also note that the overestimation of the Al *k*-ratio could be due to the effect of a native oxide layer on the Al standard and C contamination on the O standard (Fe_2O_3) (see section 4.2.5).

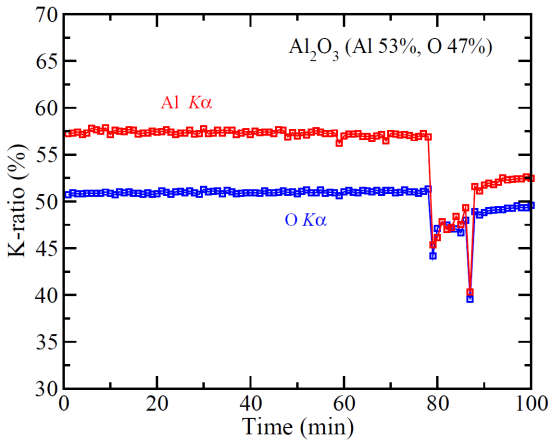

Figure 7. *k*-ratio for Al and O, as a function of irradiation time, measured on a Al_2O_3 insulator sample. Beam energy and beam current are 2.5 keV and 500 nA, respectively.

4. Factors affecting the accuracy of low-voltage EPMA

In this section, the experimental and analytical difficulties that may affect the accuracy of quantitative EPMA analysis at low voltage and the steps taken to overcome them are discussed. These include difficulties associated with the measurement of X-rays, sample characteristics, matrix correction procedures and chemical bonding effects [12].

4.1. Spectroscopic difficulties

In conventional EPMA, different X-ray lines can be selected to analyze most elements. For example, the first series of transition metals can be analyzed using their K- or L-lines. In general, K-lines are preferred because the K X-ray yield is typically one order of magnitude higher than the L X-ray yield, and because the MACs are lower. However, at low voltage, the available X-ray lines reduce to the less intense L- or M-lines. These limitations affect the accuracy of quantitative results.

Figure 8a compares portions of X-ray spectra emitted from the rutile phase of the hematite-ilmenite-rutile sample, acquired at 2.5 keV, using and not using an O_2-jet. In both cases, the C coating was removed before the measurements by in-situ etching (see section 4.1.4), in the attempt to minimize X-ray absorption (at 2.5 keV, a 25 nm thick C coating would reduce the emitted X-ray intensity by 50 %). Due to their low fluorescence yields, the intensity of the two visible Ti L-lines is even lower than that of O Kα, in spite of the higher concentration of Ti in rutile (~ 60 wt%) relatively to O (~ 40 wt%). The spectrum acquired with an O_2-jet provides better peak-to-background ratios and reduces the spectral overlap caused by the C K-line (from contamination layer). Yet, the M-lines of Zr and Nb are not observed, even at a Nb-concentration of 2 wt%.

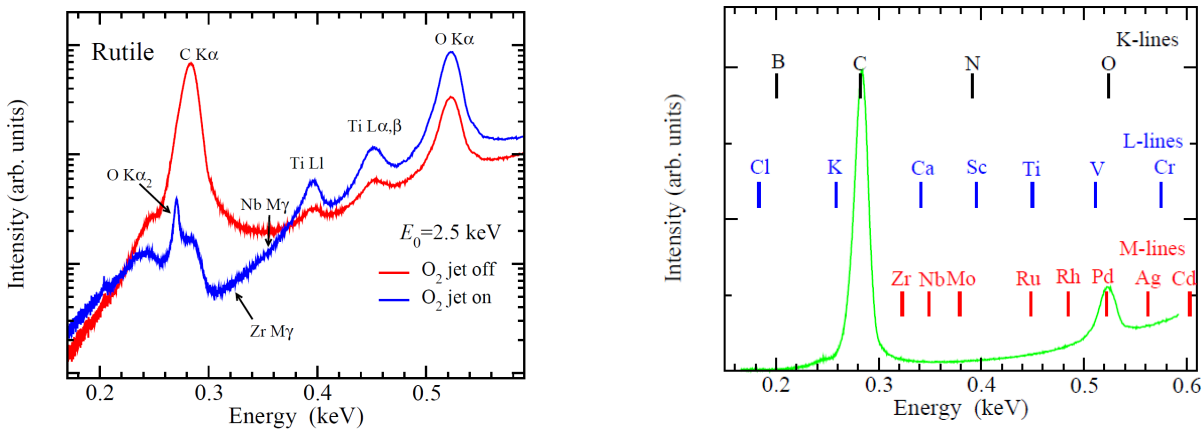

Figure 8. X-ray spectra emitted from a rutile sample (a) and from a freshly polished Zr standard (b). In the latter case, the different K-, L-, and M-lines available in the considered photon energy range are also displayed. The spectra were obtained on a Cameca SX-100 electron microprobe at an incident electron beam of 2.5 keV, using a Ni/C multilayer crystal (2d = 9.5 nm) and a 90 % Ar - 10 % CH_4 flow proportional counter, equipped with a polypropylene window, and operated at 1 bar of pressure.

A portion of the X-ray spectrum emitted from a freshly polished Zr standard obtained at 2.5 keV is shown in figure 8b, together with the energy positions of all K-, L- and M-lines that are available in the considered energy range (0.2 - 0.6 keV). Notice that, despite the use of a wavelength-dispersive (WD) X-ray spectrometer, the Zr M-lines are not detected due to the combined effect of high absorption plus extremely low fluorescence yield. Only two lines are visible in the spectrum, which correspond to C and O Kα X-rays from C contamination and oxidation layers (no anti-contamination devices were used during the acquisition). Obviously, the presence of these two lines compromises

the sensitivity of the technique. In general, since the available X-ray lines will be located at a narrow photon energy range, low-voltage EPMA will require the use of high resolution X-ray spectrometers.

At high voltages (E_0 > 15 keV), the peak-to-background ratio (P/B) ratio is relatively high and allows the determination of trace elements (with concentration less than 0.001 wt%) within reasonable counting times (t < 500 s). However, at low voltages, the P/B drops significantly and leads to worse detection limits. This is illustrated in figure 9, which shows the variation of the peak intensity and the P/B ratio for Fe Lα X-rays emitted from Fe as a function of the over-voltage ratio.

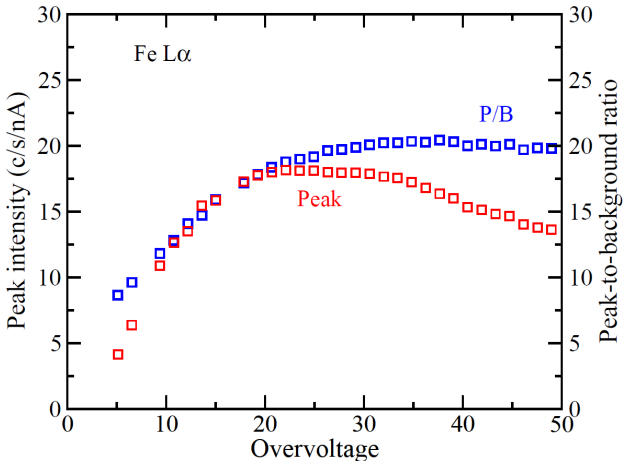

Figure 9. Variation of the peak and peak-to-background ratio (P/B) as a function of over-voltage ratio, for Fe Lα X-rays emitted from Fe.

4.2. Sample characteristics

At low voltage, a surface layer of several nanometres in thickness represents a large fraction of the sample and, therefore, the influence of hydrocarbon contamination, surface oxidation, and the quality of the sample polish becomes more significant than at higher voltages. A surface contamination layer may grow relatively fast on a freshly polished specimen at a vacuum of 10^{-5} Pa. As shown in figure 8b, the interfering effect of the C and O X-ray peaks, which correspond to contamination layers, is not negligible. Other sample characteristics such as roughness, insulator character and crystallographic orientation may also be important, as discussed below.

4.2.1. Hydrocarbon contamination. Carbon contamination occurs when hydrocarbon molecules present in the chamber are polymerized by the electron beam at the sample surface. The resulting polymer grows during electron irradiation because of its low vapour pressure and low surface mobility. The hydrocarbon molecules may originate from different instrumental sources (pump oil, vacuum grease, O-ring seals, etc.), the specimen itself, or they can also be introduced during sample preparation, storage or transportation in the air. Specimen hydrocarbon contamination typically diffuses towards the edge of the irradiated area and forms a “ring” around the beam point of impact. Beam-induced contamination is difficult to avoid even by improving the chamber vacuum (in terms of lower chamber pressure and lower hydrocarbon contents). Several techniques have been proposed to reduce carbon contamination, both at the specimen preparation stage and during measurements [13]:

1. Clean the specimen with detergent or carbon dioxide snow.
2. Heat the specimen with an electric lamp in air or in vacuum in order to desorb hydrocarbons from its surface.
3. Sputter away the surface layer in plasma cleaner.
4. Nitrogen purging of the specimen holder and specimen chamber.
5. Flood the surrounding area with electrons by defocusing the electron beam or by scanning at lower magnification in order to polymerize the surface hydrocarbons and prevent them to diffuse around the focused probe.

6. Flood the area with a gas (O_2, Ar, N_2) jet device so as to desorb hydrocarbons from its surface and keep a low hydrocarbon concentration during the measurement. This is the principle exploited by electron beam induced etching (EBIE), to etch sub-µm structures (see below), and electron-beam-induced deposition (EBID), to build sub-µm structures [14].
7. Use a N_2 cold finger in the chamber to condense hydrocarbons out of the specimen.

Figure 10 shows an example of the use of EBIE to improve the accuracy of EPMA at low voltage. In this example, an O_2-jet at a pressure of 4.10^{-4} Pa was used, together with a 2.5 keV electron beam of 500 nA and 50 µm in diameter, to etch a 25 nm thick C layer deposited on an hematite sample (Fe_2O_3). The etching rate was approximately 0.16 nm/min for a surface of 2000 μm^2. EBIE is based on the interaction of the incident and the emitted secondary electrons with the surface atoms in the presence of a precursor gas. The etching rate depends on different factors such as beam energy, current and size, temperature of the substrate material, chamber pressure, and geometry of the gas injector. EBIE is more efficient at low beam energies (~ 2 - 3 keV) because of the high yield of secondary electrons, whose contribution is dominant. As shown in figure 10, EBIE is time consuming for a large area, but the efficiency increases for smaller areas.

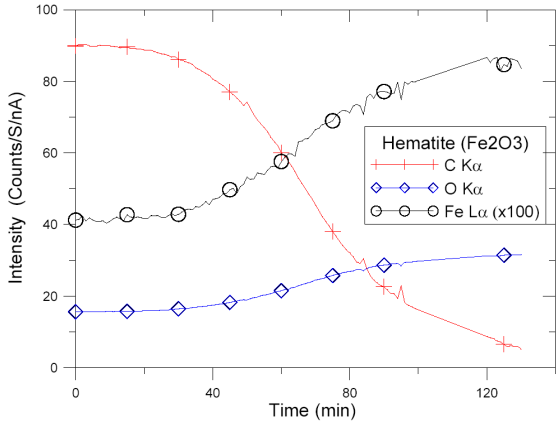

Figure 10. Electron-beam-induced etching (EBIE) of a C coated, hematite sample (Fe_2O_3) using an O_2-jet on an electron microprobe. The thickness of the C coating is 25 nm. Beam conditions: energy 2.5 keV, current 500 nA and diameter 50 µm.

Even if the EBIE technique is applied, it is useful to measure the C Kα X-ray line simultaneously with the X-ray lines of interest in order to take into account the effect of any residual C layer by using a thin-film programme.

4.2.2. Surface oxidation. Sample surface oxidation occurs in non-oxide samples. A variety of techniques can be used to reduce this effect, both at the specimen preparation and measurement stages:

1. Use freshly polished samples and standards (whenever possible).
2. Sputter away the surface layer with Ar or N_2 plasma cleaner.
3. Flood the area with a gas (N_2, Ar) jet device simultaneously with a low beam energy and high beam current in order to etch the oxidation layer using the EBIE principle.

Here it is useful to measure the O Kα X-rays simultaneously and use a thin film programme to take into account the effect of any residual oxidation layer.

4.2.3. Roughness. As discussed by Sorbier et al. [15], the uncertainties arising from sample roughness become more important at low voltage. By means of Monte Carlo simulations, these authors showed that a roughness of 10 % of the X-ray range leads to an error of 1% in the resulting concentration.

4.2.4. Insulator character. In conventional EPMA, insulating samples are routinely coated with a conductive layer [22] in order to neutralize the injected charge from the beam, with almost no influence on the evaluated composition. However, at low voltage, the energy loss of electrons in the

conductive layer can be relatively important, especially when the overvoltage is low, and it can even hinder the detection of some elements. Measurements at multiple voltages may provide the information required to separately characterize an insulator sample from the conductive coating layer.

4.2.5. Crystallographic orientation. The influence of the crystallographic orientation on the X-ray yield is usually disregarded in conventional analysis conditions. However, Meisenkothen et al. [16] have shown that at low overvoltage ratios, electron channelling may produce X-ray variations as large as 25 %, which will obviously affect the accuracy of quantitative analysis.

4.3. Limitations of quantitative procedures

Quantitative EPMA at low voltage follows the same methodology as conventional EPMA. The starting point of quantitative methods is to establish a relation between the concentration of the element of interest C_A and the measured X-ray intensity I_e. This relationship can be written as:

$$I_e = C_A . \frac{N^o}{A} . n . \frac{\Omega}{4\pi} \varepsilon . \omega_j P_{nl} . (1 + T_{CK}) . \frac{1}{\cos \alpha} . Q_l^A (E_o) . \left(\int \phi(\rho z) . \exp(\chi \rho z) . d\rho z \right) \left(1 + \sum f_c + f_{FC} \right) \quad (3)$$

where $N°$ is the Avogadro number, A is the atomic weight, n is the number of incident electrons, Ω is the solid angle of detection, ε is the detector efficiency, ω_j is the fluorescence yield, P_{nl} is the weight of the line, $(1+T_{CK})$ is a factor that takes into account Coster-Kronig transitions, α is the sample tilting angle, $Q_l^A(E_o)$ is ionisation cross-section, E_o is the accelerating voltage, E_j is the excitation energy, $\phi(\rho z) = f\left(E_o, E_j, \alpha, \sum C_i\right)$ is the depth-distribution of X-rays, $\chi = {}^{\mu}\!/_{\rho} \cos ec(\theta)$, where ${}^{\mu}\!/_{\rho}$ is the MAC and θ the take-off angle, and $\left(1 + \sum f_c + f_{FC}\right)$ is a factor that corrects for characteristic and continuum fluorescence effects.

In practice, a number of analytical, approximate expressions have been proposed to parameterize the $\phi(\rho z)$ function. These parameterisations employ quadrilateral, Gaussian, parabolic or exponential functions, which can be easily integrated to obtain C_A from I_e. The analytical $\phi(\rho z)$ expressions are defined by a few parameters (such as its maximum or its value at the surface $\phi(0)$), which depend on E_0, Z, E_i, α, and sample composition, and are usually computed from physical quantities and/or fits to experimental or Monte Carlo simulation data. To improve the accuracy of quantitative analysis, some $\phi(\rho z)$ models have been refined by imposing the qualification that the integral of $\phi(0)$ should be equal to the number of ionisations. This condition can be written as:

$$I_0 = Cst . C_A \frac{N_o}{A} . \frac{R}{S} = Cst . C_A \frac{N_o}{A} Q_l^A (E_o) . \int \phi(\rho z) . d\rho z \,, \quad (4)$$

where R and S are the backscattering and stopping power factors, respectively. Figure 11 shows the $\phi(\rho z)$ function for an Al target at 15 keV, for different excitation energies. We can see that the shape of this distribution changes rapidly with excitation energy (over-voltage ratio).

$\phi(\rho z)$ models adopt simple expressions for the calculation of R, S and Q (E_0). For example, S is generally computed by using the Bethe formula and Q (E_0) is also determined by means of the Bethe ionisation cross-section (see e.g., [18]). Although these formulas have been often tuned [23] to provide the best match between the predicted X-ray intensities and selected experimental measurements, their validity at low incident electron energies is not firmly established. This is illustrated in figure 12, which compares different calculations and experimental measurements of the cross section for the production of Au Mα X-rays and the stopping power for Cu. In the case of the ionisation cross-section (figure 12a), the experimental measurements are only reproduced by the most

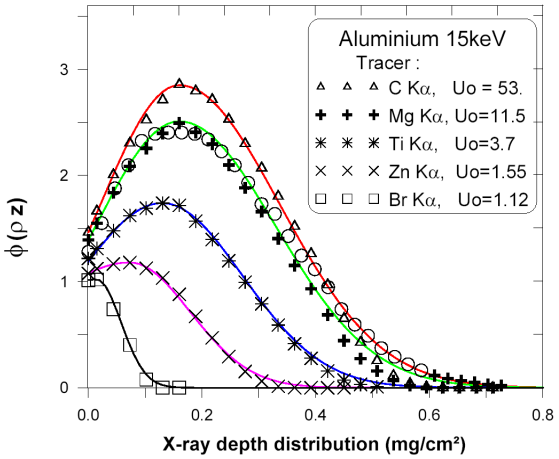

Figure 11. Depth-distribution of X-ray production for various X-ray lines (tracer elements) in Al at 15 keV. Circles are experimental measurements of Castaing and Hénoc [17]; other symbols are Monte Carlo simulation results; continuous lines are the predictions of the X-PHI model [7].

sophisticated calculation based on the distorted-wave Born approximation (DWBA) [19], whereas the Bethe-Powell formula, as well as other predictive formulas widely used in EPMA, systematically underestimate the experimental data especially near the ionisation threshold. As for the stopping power, this can be evaluated by using the Bethe formula only for electrons with energy larger than the excitation energy of the most tightly bound shell (figure 12b).

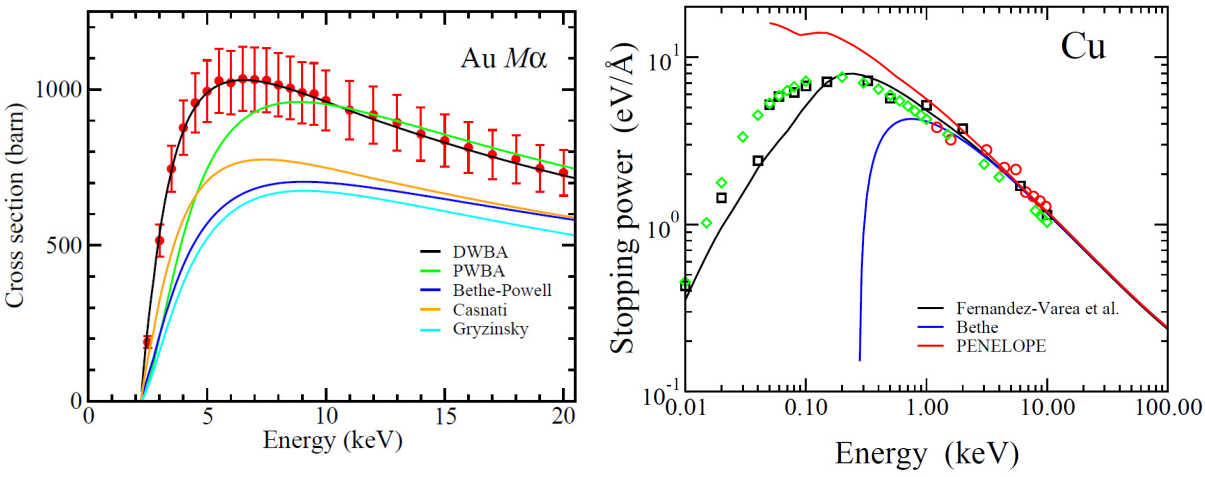

Figure 12. Cross-section for the production of Au Mα X-rays (a) and stopping power of electrons in Cu (b). Continuous lines are the results of different calculations and predictive formulas, some of them widely used in EPMA. Symbols are experimental data taken from the literature.

Recent measurements of the surface ionisation $\phi(0)$ for L- and M-shells [20] have shown the limitations of currently available EPMA models for such lines at low energies. While the more sophisticated calculations performed with the Monte Carlo simulation code PENELOPE [20], which adopts ionisation cross-sections computed from the DWBA, were found to reproduce the measured $\phi(0)$ values reasonably well, none of current available $\phi(0)$ parameterisations was found to reproduce consistently the experimental data [20].

4.4. Chemical bonding

X-ray emission lines that correspond to electron transitions involving outer valence electrons are known to be sensitive to chemical bond [24]. As a result, a shift in peak position as well as a change in peak distribution is observed when comparing X-ray lines of the same element in different chemical environments. For some low-energy lines, such as the L-lines of the first series of transition elements, the chemical state of the transition atom may also be responsible for changes in the X-ray distribution as well as in the self-absorption. The use of empirical MACs obtained from EPMA measurements at variable voltage may be useful to overcome these difficulties.

Conclusions

Low-voltage EPMA offers advantages for the characterisation of thin films and multilayers, ultra-light elements and insulators, but more importantly, it opens a wide range of new possibilities for the characterisation of materials that are heterogeneous on a sub-micrometre scale. However, low-voltage EPMA is affected by experimental and analytical difficulties that deteriorate the accuracy of quantitative results and requires a more careful approach than conventional EPMA.

The recent improvements in EPMA instrumentation represent a major step towards the application of EPMA at low voltage on a routine basis. Nevertheless, further studies must still be made in order to improve the reliability of quantification models at such energy range. It is to be hoped that these studies will provide improved sets of fundamental parameters, such as MACs, ionisation cross-sections, fluorescence and Coster-Kronig yields and stopping powers, consistent with EPMA models and suitable for low-voltage applications.

Acknowledgements

We would like to thank Fernanda Guimarães and Michel Outrequin for performing the X-ray maps on the FEG EPMA instruments.

References

[1] Newbury D E 2002 *J. Res. Natl. Inst. Stand. Technol.* **107** 605-19
[2] Cazaux J 2010 *J. Electron Spectros. Rel. Phenomena* 176 58-79
[3] Willich P and Bethke R 1996 *Mikrochim. Acta* Suppl. **13** 631-8
[4] Llovet X and Merlet C 2010 *Microsc. Microanal.* **16** 21-32
[5] Castaing R 1952 Ph.D-thesis. Publication ONERA no. 55
[6] Bastin G F, Dijkstra J M, Heijligers H J M and Klepper D 1993 *Microbeam Anal.* **2** 29
[7] Merlet C 1994 *Mikrochim. Acta* **114/115** 363
[8] Henke B L, Gullikson E M and Davis J C 1993 *Atom. Data Nucl. Data Tables* **54** 181
[9] Kalfoun F, Ionov D and Merlet C 2002 *Earth Planet. Sci. Lett.* **199** 49-65
[10] Pascal C, Merlet C, Marin-Ayral R M, Tédenac J C and Boyer B 2004 *Mikrochim. Acta* **145** 147-51
[11] Llovet X and Galan G 2003 *Am. Mineral.* **88** 121
[12] Llovet X, Heikinheimo E, Núñez A, Merlet C, Almagro J F, Richter S, Fournelle J, van Hoek C J G 2012 *IOP Conf. Ser.: Mater. Sci. Eng.* **32** 012014
[13] Egerton R F, Li P and Malac M 2004 *Micron* **35** 399-409
[14] Randolph S J, Fowlkes J D and Rack P D 2006 *Crit. Rev. Solid State Mater. Sci.* **31** 55-89
[15] Sorbier L, Rosenberg E and Merlet C 2004 *Micros. Microanal.* **10** 745-52
[16] Meisenkothen F, Wheeler R and Uchic M D 2009 *Microsc. Microanal.* **15** 83-92
[17] Castaing R and Hénoc J 1965 *Proc. 4th IXCOM.* Castaing R, Deschamps P and Philibert J, eds. (Paris: Hermann) pp. 120
[18] Salvat F, Llovet X and Fernández-Varea J M 2004 *Microchim. Acta* **145** 193-202
[19] Bote D and Salvat F 2010 *Phys. Rev. A* **77** 042701
[20] Merlet C and Llovet X 2011 *X-ray Spectro.* **40** 47-54

[21] Salvat F, Fernández-Varea J M and Sempau J 2009 *PENELOPE-2008: A code system for Monte Carlo simulation of electron and photon transport.* (Issy-les-Moulineaux, France: OECD/NEA Data Bank)
[22] Cazaux J 2004 *Microsc. Microanal.* **10** 670-84
[23] Joy D 1998 *J. Micros.* **191** 74-82
[24] Remond G, Gilles C, Fialin M, Rouer O, Marinenko R, Myklebust R and Newbury D 1996 *Mikrochim. Acta* Suppl. **13** 61-86